A Compact I-V Model for FinFETs Comprising Multi-Dimensional Electrostatics and Quantum Mechanical Effects

D. Zhang, Z. Yu and L. Tian

Institute of Microelectronics, Tsinghua University
Beijing, China, zdw99@mails.tsinghua.edu.cn

ABSTRACT

A compact *I-V* model for FinFET using ballistic transport with 1D electron gas is presented. The 2D electrostatics and 2D quantum mechanical (QM) effects at the cross-section are fully taken into account, which ensures the applicability to various types of FinFETs, from double-gate (DG) to Omega FinFET or nanowire FinFET. Compared to numerical simulations and experimental data, the model correctly predicts carrier density and terminal current of decanano-scaled devices.

Keywords: compact *I-V* model, FinFET, 2D quantum mechanical effects

1 INTRODUCTION

Continually scaling has driven conventional CMOS devices into a dilemma due to electrostatic concerns (high leakage current) [1]. One of the most promising substitutes beyond 65nm node may be the FinFET thanks to its superior characteristics and relatively compatible technology [2-4]. Thus, compact models for such devices are desirable for the next generation circuit design. There have been extensive works on this field [5-7]. However, they all focus on the electrostatics along the channel and the width direction, thus applicability being restricted to DG-MOSFETs since the effect of the top gate is neglected. Moreover, the QM effects, which play an essential role in the practical FinFETs with deca-nano scaled widths, are ignored. In [8-9], QM effects are comprised while modeling. However, the work is either over-simplified (with a box-like flat potential well, limiting the model can only be applied to a device with ultra-thin width) [8] or too complicated to be applied for compact modeling [9]. Plus, only 1D QM effects along the width direction are considered, which is insufficiently for tri-gate devices.

In this work, both the 2D electrostatics and the 2D QM effects at the cross-section of a FinFET are comprised while modeling carrier density, ensuring the model capable of applied to devices with a wide range of fin widths and fin heights. With the fin width and height changing from ultra-low (say 5nm) to relatively-high (say deca-nano scale), the mechanism that the carriers in the channel shift from body inversion (such as nanowire case) to surface conductance (such as nanotube case) is fully incorporated into the compact model. Furthermore, utilizing ballistic transport [10] with 1D electron gas and considering all the subbands in all the valleys, a compact I-V model is finally completed. This model may be applicable for the practical FinFETs of various types with an arbitrary deca-nano scaled channel length, width and height.

2 CHARGE MODEL

A diagram of the cross-section of a FinFET is depicted in Fig. 1 for convenience.

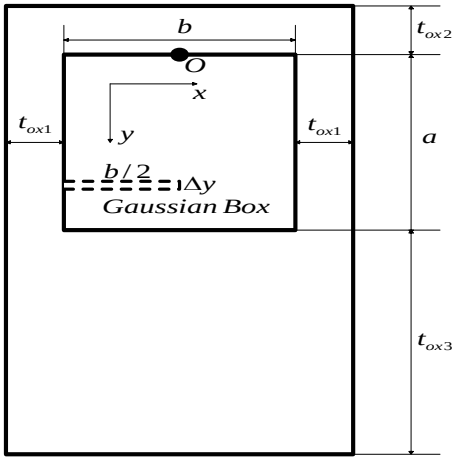

Figure 1: Diagram of the cross-section of a FinFET. Channel width: b, channel height: a, side-gate oxide thickness: t_{ox1}, top-gate oxide thickness: t_{ox2}, buried oxide thickness: t_{ox3}

Applying Gauss' Law to a 2D rectangular box (Gaussian box in Fig. 1) and noticing the displacement flux continuity at the interfaces, one obtain the following equation:

$$\frac{d^2\phi(0,y)}{dy^2}+\frac{8C_{ox1}}{b^2\left(C_{ox1}+C_d\right)}\left[V_G-\left(\phi_M-\chi\right)-\phi(0,y)\right]=\frac{q\left(N_e+N_A-N_D\right)}{\varepsilon_{si}} \quad (1)$$

With $\phi(0,y)$ electric potential. All the other notations can be found in [8]. Using the boundary conditions along height direction, Eq. (1) yields an expression of $\phi(0,y)$ as a function of gate voltage and electron density (for details see [11]).

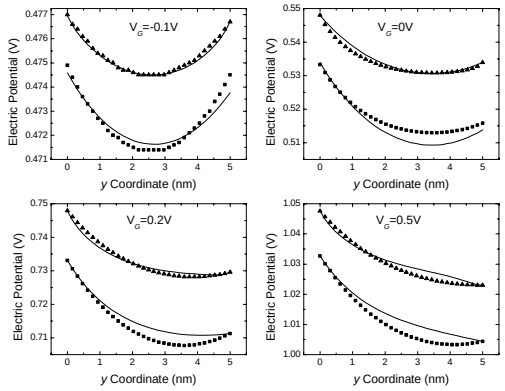

Figure 2: $\phi(-b/2,y)$ and $\phi(0,y)$ at various gate voltages. $a=b=5\text{nm}$, $t_{ox1}=t_{ox2}=1\text{nm}$ and $t_{ox3}=25\text{nm}$. Symbols stand for numerical simulation results (triangles: $\phi(-b/2,y)$, squares: $\phi(0,y)$) while lines stand for analytical results.

Fig. 2 shows the consistency between analytical profiles and numerical ones (using DESSIS [12]). Defining ϕ_c as the minimum potential at the cross-section, i.e. the potential at the position where $d\phi(0,y)/dy=0$, one derives the relation among charge density, effective gate bias $V_G^{'}$ [8] and ϕ_c (detailed process is published in another paper [11]):

$$\left|Q_{e_line}\right| = 2C_g\left(V_G^{'}-\phi_c\right)/H \qquad (2)$$

With C_g gate capacitance [8] and $H=1+E/F\left(e^{-a/D}-2e^{-a/2D}\sqrt{\cosh(a/D)}\right)$, denoted as "tri-gate coefficient", where D, E and F have explicit forms of a,b,t_{ox1},t_{ox2} and t_{ox3}. H is a critical parameter to reflect the 2D electrostatics and always stays lower than unity. In Fig. 3, H is depicted against a.

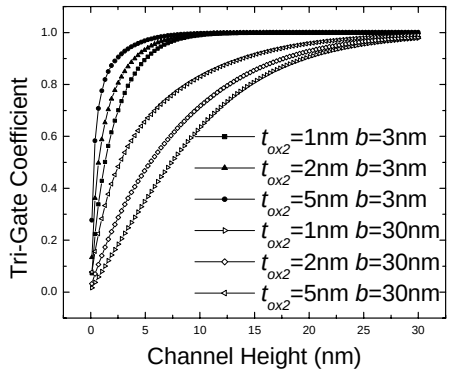

Figure 3: Tri-gate coefficient H versus channel height a with different t_{ox2} and b. $t_{ox1}=1\text{nm}$ and $t_{ox3}=30\text{nm}$.

With an increasing channel height, H increases, indicating weaker top-gate control ability, and gradually approaches to unity, leading Eq. (1) to DG-MOSFET case, consistent with that in [8]. Also, with increasing t_{ox2} or decreasing b, H increases, indicating a declining control ability of the top-gate.

On the other hand, using the density-of-states of 1D electron gas N_{1D} and Fermi-Dirac statistics, the charge line density may be expressed as:

$$\left|Q_{e_line}\right| = \sum_{n_x=1}^{N_x}\sum_{n_y=1}^{N_y}\sum_{k=1}^{N_v} qN_{1D}\zeta_{-1/2}\left[-\left(E_{n_x,n_y,k}-q\phi_c-E_{Fn}\right)/k_BT\right] \qquad (3)$$

Summed up with different quantum numbers in two directions n_x and n_y and different valleys k. $\zeta_{-1/2}$ is the negative half order of the Fermi integral, $E_{n_x,n_y,k}$ is the eigen-energy with the reference $E_{c0}=-q\phi_c$ and E_{Fn} is the quasi-Fermi level. The importance of 2D QM effects lies in deriving a correct analytical expression of $E_{n_x,n_y,k}$. We use separate variable method to respectively obtain the energy along two directions. A qualitative diagram for energy levels along width direction is plotted in Fig. 4.

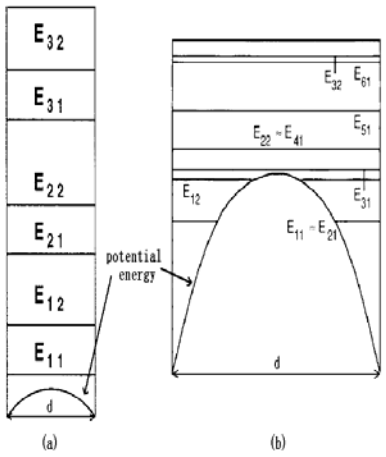

Figure 4: Qualitative diagrams of energy levels in the potential well along width direction. A narrower width is assumed on the left while a wider width on the right.

If the width is ultra-narrow, the lowest energy is above the potential energy and the potential energy may be regarded as perturbation. With an increasing width, the energy levels decrease, finally drop into the two triangle-like potential wells. Therefore, a strategy is developed to estimate the energy levels: respectively calculate the analytical values for the square potential well with 1st order perturbation and those for the triangle potential well [13], then select which one to use according to the criterion shown in Fig. 5.

If $E_{n,k_squ} < E_{n,k_tri}$	
then	$E_{n,k_ana} = E_{n,k_squ}$
Else if $E_{n,k_squ} > 0$ (using $E_{n,k_tri} > 0$ for height direction)	
then	$E_{n,k_ana} = E_{n,k_squ}$
Else	
then	$E_{n,k_ana} = E_{n,k_tri}$

Figure 5: Strategy for obtaining energy levels E_{n,k_ana} from the combination of those from triangle well E_{n,k_squ} and those from square well with 1st order perturbation E_{n,k_tri}.

In Fig. 6, the analytical results and the numerical simulations from Shred 2.0, strictly solving Schrödinger equation [14], of the electron density are shown.

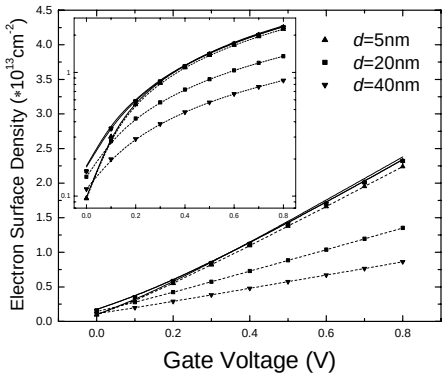

(a)

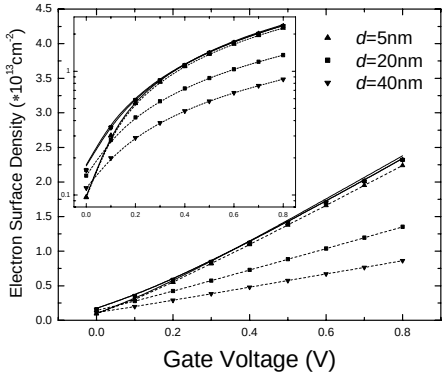

(b)

Figure 6: Electron surface density versus gate voltage with different channel widths (a) and oxide thickness (b) on linear scale and logarithmic scale. Symbols: the numerical results. Lines: analytical results fully comprising QM effects. Dashed lines with symbols: analytical results with box-like-potential [8].

Clearly, our model predicts the same trend as numerical. The model barely considering a box-like potential [8], however, underestimates the electron density and the error increases with an increasing width. The calculation of energy levels along height direction is similar with that of width direction. The only difference is that the potential well is asymmetric, which causes the criterion to be adjusted (the adjustment is shown in the bracket in Fig. 5). Now that $E_{n_x,n_y,k}$ is obtained, equating Eq. (1) and (3), one may obtain an implicit form of charge density. Executing the similar procedure in [8], one may finally derive an explicit form of charge density as (valid both in weak and strong inversion):

$$\left|Q_{e_line}\right| = \frac{2C_g a k_B T}{qH} \log\left\{1+\exp\left[q\left(V_{GS}-V_T-V\right)/k_B T\right]\right\} \quad (4)$$

with $V_T = \phi_M - \chi + (N_A - N_D)2C_g/H + \frac{k_B T}{q}\log\left(2C_g a k_B T/q^2 N_c' H\right)$ the threshold voltage and $N_c' = \sum_{n_x=}^{N_x}\sum_{n_y=1}^{N_y}\sum_{k=1}^{N_z} N_{1D}\exp\left(-E_{n_x,n_y,k}/k_B T\right)$ the effective density of states incorporating the 2D QM effects.

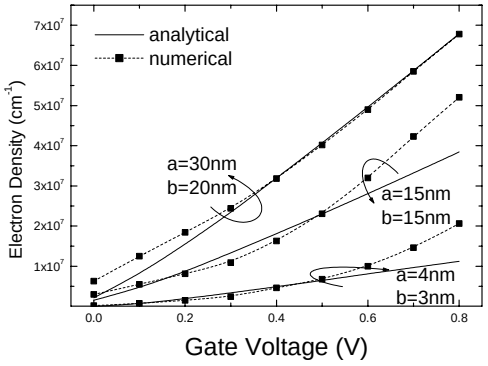

Figure 7: Electron Line Density versus gate voltage with different widths and heights.

In Fig. 7, the analytical electron line density shows good accordance with the numerical results from Taurus with MLDA QM model [15] with different widths and heights of deca-nano scale. The threshold voltage decreases with an increasing channel width, shown in Fig. 8. The QM model, only considering box-like potential, slightly overpredicts V_T.

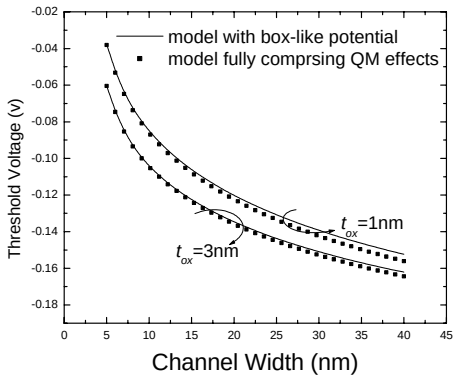

Figure 8: Threshold voltage versus channel width with different gate-oxide thickness.

3 *I-V* MODEL

In [10], modeling for ballistic transport is presented. But it is only capable for ultra-thin body DG-MOSFET because 2D electron gas is assumed, which is not the case for nanowire FinFETs where carriers are confined in both directions vertical to channel, and only the lowest subbands of the unprimed valleys are considered, which restricts the applicability to the ultra-thin devices. In this work, all the valleys are considered with the drain current calculated as $I_{DS} = \sum_{k=1}^{N_v} I_{DS,k}$, where $I_{DS,k}$ has the similar form of Eq (6) in [10] except that all the Fermi Integrals lower by half an order, indicating the difference of the density of states between 1D and 2D electron gas. Besides, the summations of all subbands are performed while calculating those Fermi integrals.

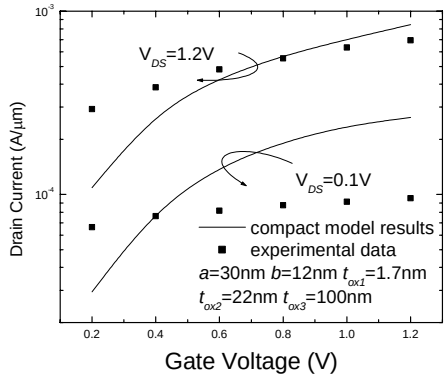

Figure 9: Drain current versus gate voltage under different drain bias. The device structure is from [2].

In Fig. 9, the transfer characteristics calculated by our model of a 10nm FinFET [2] are depicted, showing satisfactory consistency with the measured data [2].

4 CONCLUSION

A compact I-V model for FinFETs of deca-nano scale is developed comprising 2D electrostatics, 2D QM effects and ballistic transport. Its applicability is proved by numerical simulations and experimental data.

REFERENCES

[1] The ITRS 2001. http://public.itrs.net.
[2] Bin Yu et al., "FinFET Scaling to 10nm Gate Length," *IEDM Tech Digest*, 2002
[3] Fu-Liang Yang et al., "5nm-Gate Nanowire FinFET," Symp. VLSI Tech., 2004
[4] Yang-Kyu Choi et al., "Sub-20nm CMOS FinFET Technologies," IEDM *Tech Digest*, 2001
[5] Qiang Chen et al., "A Physical Short-Channel Threshold Voltage Model for Undoped Symmetric Double-Gate MOSFETs," Trans. Electron Devices, Vol.50, pp. 1631-1636, 2003
[6] Gen Pei et al., "A Physical Compact Model of DG MOSFET for Mixed-Signal Circuit Applications—Part I: Model Description," Trans. Electron Devices, Vol. 50, pp. 2135-2153, 2003
[7] Xiao P. Liang et al., "A 2-D Analytical Solution for SCEs in DG MOSFETs," Trans. Electron Devices, Vol. 51, pp. 1385-1391, 2004
[8] Giorgio Baccrani et al., "A Compact Double-Gate MOSFET Model Comprising Quantum-Mechanical and Nonstatic Effects," Trans. Electron Devices,Vol.46,pp.1656-1666,1999
[9] Lixin Ge et al., "Analytical Modeling of Quantization and Volume Inversion in Thin Si-Film DG MOSFETs," Trans. Electron Devices, Vol. 49, pp. 287-294, 2002
[10] A. Rahman et al., "A compact scattering model for the nanoscale double-gate MOSFETs," Trans. Electron Devices, Vol. 49, pp. 481-489, 2002
[11] D. Zhang et al., "A Compact Threshold Voltage Model for FinFETs," Chinese Journal of Semiconductors, to be published.
[12] http://www.ise.ch ISE 8.0 User Manual.
[13] Yutao Ma et al., "Validity and Applicability of Triangular Potential Well Approximation in Modeling of MOS Structure Inversion and Accumulation Layer," Trans. Electron Devices, Vol. 47, pp. 1303-1305, 2000
[14] http://www.nanohub.purdue.edu/NanoHub/.
[15]http://www.synopsis.com/support/support_ctr Taurus User Manual.